Environmental Science & Technology

Article

pubs.acs.org/est

Fate of Adsorbed U(VI) during Sulfidization of Lepidocrocite and Hematite

Vasso G. Alexandratos,*[†] Thilo Behrends,[†] and Philippe Van Cappellen[‡]

[†]Faculty of Geosciences, Utrecht University, P.O. Box 80.021, 3508 TA Utrecht, The Netherlands

[‡]Ecohydrology Research Group, Water Institute and Department of Earth and Environmental Sciences University of Waterloo, 200 University Avenue West, Waterloo Ontario Canada

Supporting Information

ABSTRACT: The impact on U(VI) adsorbed to lepidocrocite (γ-FeOOH) and hematite (α-Fe_2O_3) was assessed when exposed to aqueous sulfide ($S(-II)_{aq}$) at pH 8.0. With both minerals, competition between S(-II) and U(VI) for surface sites caused instantaneous release of adsorbed U(VI). Compared to lepidocrocite, consumption of $S(-II)_{aq}$ proceeded slower with hematite, but yielded maximum dissolved U concentrations that were more than 10 times higher, representing about one-third of the initially adsorbed U. Prolonged presence of $S(-II)_{aq}$ in experiments with hematite in combination with a larger release of adsorbed U(VI), enhanced the reduction of U(VI): after 24 h of reaction about 60−70% of U was in the form of U(IV), much higher than the 25% detected in the lepidocrocite suspensions. X-ray absorption spectra indicated that U(IV) in both hematite and lepidocrocite suspensions was not in the form of uraninite (UO_2). Upon exposure to oxygen only part of U(IV) reoxidized, suggesting that monomeric U(IV) might have become incorporated in newly formed iron precipitates. Hence, sulfidization of Fe oxides can have diverse consequences for U mobility: in short-term, desorption of U(VI) increases U mobility, while reduction to U(IV) and its possible incorporation in Fe transformation products may lead to long-term U immobilization.

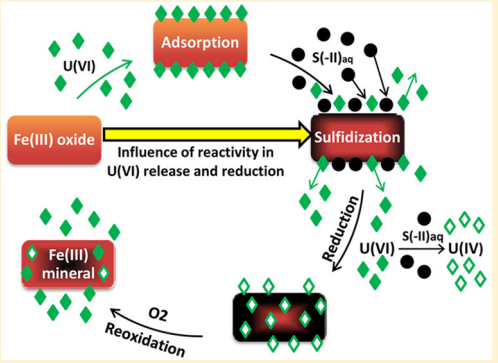

1. INTRODUCTION

Uranium-contaminated sites, a legacy of uranium (U) mining and processing,[1−4] are an environmental concern because U poses health risks as a heavy metal and a source of radioactive radiation.[5−8] The fate of U in the environment is often linked to the biogeochemistry of iron (Fe) via sorption and redox processes. For example, the mobility of U can be determined by a variety of interactions with iron oxides (here collectively referring to iron oxides, iron hydroxides, and iron oxy-hydroxides), including (a) Adsorption of hexavalent uranium (U(VI)), the most oxidized and soluble form of U, which occurs at the surfaces of iron oxides at fast rates and may lead to the formation of strong inner-sphere complexes,[9−13] (b) Incorporation of U(VI) into iron oxides via coprecipitation[14] or recrystallization of ferrihydrite,[15,16] (c) Reduction of U(VI) to U(IV), either mediated by iron oxides as catalytic surfaces where adsorbed Fe^{2+} acts as the reductant,[17,18] or through direct reduction by structural Fe(II) in mixed redox state iron oxides (e.g., green rust, magnetite),[19,20] and d) Reoxidation of U(IV) to U(VI) by iron oxides.[21] In the latter case, the capability of oxidizing U(IV) depends on the Gibbs energies of formation of the iron oxide and the U(IV) bearing phase.[22−24]

In subsurface environments, redox conditions may shift from oxic to anoxic and trigger microbial sulfate reduction.[25−27] Production of S(-II) causes changes in iron mineralogy, with Fe(III)-bearing minerals transforming into iron sulfides.[28−35] Sulfidization of iron oxides can affect the partitioning of previously adsorbed toxic constituents, as in the case of arsenic,[36,37] as well as their oxidation state, as in the case of reduction of arsenate by sulfide.[38] Sulfidization of U(VI)-bearing iron oxides raises the question of whether or not the released U will remain mobile.[39−41] In addition to producing new phases, such as FeS or pyrite (FeS_2),[42−44] free sulfide is capable of reducing U(VI) to U(IV). When reduction to U(IV) is followed by uraninite (UO_2) precipitation, the overall effect would be U immobilization.

The addition of aqueous sulfide ($S(-II)_{aq}$) to a suspension containing lepidocrocite (γ-FeOOH) with adsorbed U(VI) was investigated in a previous study.[45] The observed immediate release of U to solution upon $S(-II)_{aq}$ addition was interpreted as a result of S(-II) adsorption onto lepidocrocite, out-competing U(VI) for available surface sites. However, the fraction of U(VI) reduced to U(IV) only reached 50% of the total U, after 24 h of reaction. This was the case even when $S(-II)_{aq}$ was added in excess. The incomplete extent of U(VI) reduction was attributed to the rapid oxidation of $S(-II)_{aq}$ by lepidocrocite and the kinetic hindrance of reduction of U(VI) sorbed to the solids. Thus, partial U mobilization may be a

Received: November 3, 2016
Revised: January 24, 2017
Accepted: January 25, 2017
Published: January 25, 2017

DOI: 10.1021/acs.est.6b05453
Environ. Sci. Technol. 2017, 51, 2140−2150

possible outcome in environments containing U-bearing iron oxyhydroxides exposed to sulfide production.

Building on the results of Alexandratos et al.,[45] the aim of this present study was to compare the fate of U(VI) preadsorbed to lepidocrocite and hematite upon the introduction of aqueous sulfide. The two mineral phases were selected because of the markedly lower reactivity of hematite toward sulfide than lepidocrocite.[33,46] Thus, we hypothesized that the prolonged presence of dissolved S(-II) in hematite suspensions could enhance the initial desorption of U due to competition of S(-II) with U(VI) for surface sites. However, we further considered that increased desorption of U(VI) into a S(-II)-rich solution may facilitate the reduction of U(VI) by sulfide. Reaction with dissolved S(-II) was previously shown to be the most effective pathway for U(VI) reduction in experiments with lepidocrocite.[45] In the experiments presented here, suspensions of synthetic lepidocrocite and hematite with adsorbed U(VI) were exposed to different amounts of $S(-II)_{aq}$. Phase distribution of U was monitored as a function of time and X-ray absorption spectroscopy (XAS) was used to determine the redox state and speciation of solid-bound U. The goal was to assess the role of iron oxide reactivity toward sulfide in U desorption and reduction.

2. MATERIALS AND METHODS

2.1. Experimental Conditions and Reagents. With the exception of the reoxidation experiments, all experiments, sample collection and preparation of samples for X-ray absorption spectroscopy (XAS) were performed in a glovebox under a N_2 (95%) and H_2 (5%) atmosphere. The glovebox was equipped with a Pd catalyst and an O_2 monitor in order to maintain oxygen levels below 10 ppm. The temperature in the glovebox was kept constant at 25 °C. The possibility of uranium uptake by the glassware used (DURAN ISO laboratory bottles) was investigated in advance by performing repeated blank adsorption experiments: it turned out to be insignificant. Stock solutions of U(VI) and S(-II) were prepared from uranyl acetate and anhydrous Na_2S, respectively. All chemicals used were of reagent grade and no further purification was performed.

2.2. Mineral and Suspension Preparation. Synthetic lepidocrocite (γ-FeOOH) and hematite (α-Fe_2O_3) were synthesized following the procedures described in Schwertmann and Cornell.[47] Lepidocrocite was produced by oxidation of a $FeCl_2$ solution in a reactor connected to a pH-stat unit that maintained pH at 6.8 by adding 1 M NaOH. Hematite was synthesized by forced hydrolysis of Fe(III) by slowly adding 1 M $Fe(NO_3)_3$ solution to boiling water. After synthesis, the suspensions were dialyzed against deinonized water and stored as aqueous stock suspensions. Powder X-ray diffraction (XRD) did not show any mineral phases present other than lepidocrocite and hematite in the corresponding suspensions. For lepidocrocite, the N_2–BET surface area was determined as 78 $m^2\ g^{-1}$. For hematite, the peak width in XRD measurements corresponded to a particle diameter of 15 nm based on the Scherrer equation.[48] This particle size corresponds to a specific surface area of about 80 $m^2\ g^{-1}$ when assuming spherical particles.

Lepidocrocite and hematite suspensions were prepared inside the glovebox by diluting the aforementioned stock suspensions in deoxygenated distilled water. Loadings were approximately 1 g/L, corresponding to concentrations of 9.3 mM Fe_{tot} for lepidocrocite and 12.2 mM Fe_{tot} for hematite. To remove dissolved CO_2, suspensions were purged with Ar prior to use. Ionic strength was adjusted to 0.1 M by adding the required amount of NaCl. In order to keep the pH constant during the reaction, TAPS buffer (0.04 M $C_7H_{17}NO_6S$) was added and the pH adjusted to 8.0 with HCl or NaOH as necessary. A pH value of 8.0 is representative of subsurface environments in which alkalinity is produced by microbial sulfate reduction.[49] Furthermore, as the pK_a of H_2S is about one unit below pH 8.0, only about 10% of $S(-II)_{aq}$ was in the form of H_2S and outgassing did not significantly influence the amount of dissolved sulfide on the time scale of hours. Suspensions were left overnight to stabilize while stirring to maintain suspension homogeneity. Following this, U(VI) solution was added to both iron oxide suspensions, giving total U concentrations of about 12 μM with lepidocrocite and 13.5 μM with hematite suspensions, and then were left to equilibrate for 24 h.

2.3. Reduction Experiments and Sample Collection. Abiotic reduction was initiated by adding aqueous sodium sulfide (Na_2S) to the equilibrated U(VI)-bearing lepidocrocite and hematite suspensions. Suspensions were divided in three identical portions, labeled L1, L2, L3 for lepidocrocite and H1, H2, H3 for hematite, to which aqueous sulfide was added at concentrations of 10, 5, and 1 mM, respectively (Table 1). All suspensions were in closed vessels and stirred using magnetic stir bars throughout the experimental duration (72 h). To avoid sudden pH changes in the suspensions due to sulfide addition, the pH of each Na_2S injection was individually adjusted to pH 8.0 by adding the required amount of 2 N HCl. The amounts of HCl were predetermined from preliminary titrations in Na_2S solutions and corresponded to the amount of acid required to convert S^{2-} into HS^- in the injection solution.

Table 1. Sulfide and Uranium That Was Added to Lepidocrocite and Hematite Suspensions

suspension	$[U(VI)]_{tot}$ (μM)	[S(-II)] addition (mM)	$Fe(III)_{tot}$ (mM)
L1	12	10	9.3
L2	12	5	9.3
L3	12	1	9.3
H1	13.5	10	12.2
H2	13.5	5	12.2
H3	13.5	1	12.2

In order to monitor the progress of the reaction, aliquots were periodically collected by syringe starting about 2 min before sulfide addition. After filtration through 0.2 μm pore-size nylon filters, dissolved Fe(II) was measured by spectrophotometry using the ferrozine method,[50] dissolved S(-II) was trapped in zinc acetate solution and S(-II) concentration was determined by spectrophotometry using the methylene blue method,[51] and dissolved U concentrations were determined on an Agilent 4500C inductively coupled plasma mass spectrometer (ICP-MS). Prior to U measurements, the filtered solutions were diluted about 100 times with 1 M suprapure HNO_3. Additionally, at each sampling moment, an aliquot of 2 mL of the experimental suspension was taken and added to 2 mL of 12 M HCl for dissolving all solids and determining total Fe and U concentrations. The coefficients of variation of the measured total U concentrations for the different series was between 3.3% and 7.0%. Hence, 7.0% was taken as an upper limit for the uncertainty of U measurements.

DOI: 10.1021/acs.est.6b05453
Environ. Sci. Technol. 2017, 51, 2140–2150

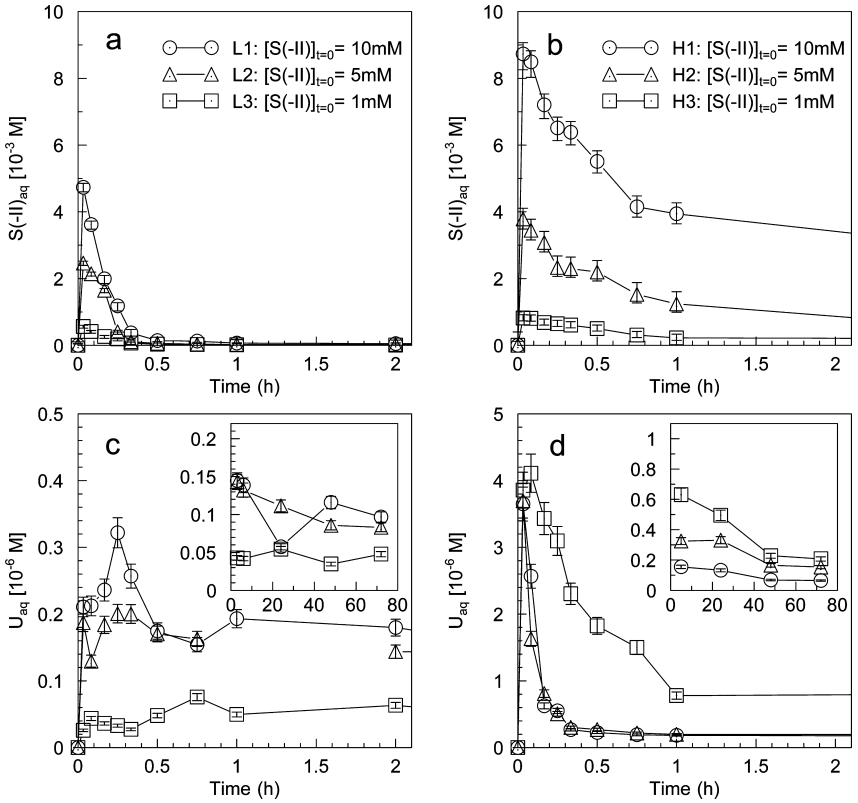

Figure 1. (a, b) Time evolution of dissolved S(-II) in (a) lepidocrocite suspensions L1, L2, and L3 and (b) hematite suspensions H1, H2, and H3, (c, d) Time evolution of dissolved uranium (U_{aq}) in (c) lepidocrocite suspensions L1, L2, and L3 and (d) hematite suspensions H1, H2, and H3, after S(-II) addition (Legends for graphs 1c and 1d follow the same symbolism as in 1a and 1b, respectively). Inlet graphs show U_{aq} concentrations for the full extent (72 h) of experimental duration. Total concentration of uranium in lepidocrocite and hematite suspensions were 12 and 13.5 μM, respectively. The error bars represent the 95% confidence interval for the S(-II) measurements and a 7% coefficient of variation for the uranium concentrations.

2.4. X-ray Absorption Spectroscopy. Solid material for XAS analysis was recovered from 100 to 150 mL of the reacting lepidocrocite and hematite suspensions. Sampling took place after 0 (just prior to sulfide addition), 2, 6, 24, 48, and 72 h of reaction with sulfide. Pore-size filters of 0.2 μm (polycarbonate, Millipore) were used to collect the solids. The wet pastes obtained from the filters were placed into the cavities of custom-made sample holders (PTFE). Each cavity was closed with Kapton tape and the sample holder was then heat-sealed in an LDPE bag. Samples were kept at −80 °C and transferred to the beamline in dry ice. X-ray absorption spectra were collected at the DUBBLE beamline (BM26a) of the ESRF in Grenoble, France. A description of the beamline and its optics is provided by Borsboom et al.[52] and Nikitenko et al.[53] Samples were installed in a cryostat (30 K) during measurement. Spectra were collected in fluorescence mode at the uranium L_{III} edge around 17.17 keV. Energy calibration was performed by adjusting the first maximum of the first derivative of the yttrium foil spectrum to 17.038 keV.

X-ray spectra were processed with the Athena software.[54] ITFA software[55] was used for the eigenanalysis of the spectra and the iterative target test (ITT). Eigenanalysis assisted in determining the number of factors that are necessary to explain the variability between the spectra. In the analysis of X-ray absorption near edge structure (XANES), the energy range for the normalized X-ray spectra was between 17.10 and 17.25 keV. For the eigenanalysis of the extended X-ray absorption fine structure (EXAFS), the k^3-weighted spectra were used in a k-range between 2 and 10 $Å^{-1}$. The ITT analysis was applied to extract real end-member spectra from the data set and to calculate the relative concentrations of the different components in the various samples. The advantage of using ITT analysis in comparison to linear combination fitting is that the endmember spectra do not have to be defined a priori but are extracted from the data set. However, after sulfide addition, the suspension most likely contained uranium in different oxidation states and none of the spectra represents a pure endmember spectrum of uranium in the form of U(IV). For this reason, the set of XANES spectra was complemented with the spectrum of a U(IV) standard. By this, the component, extracted in the ITT analysis for the reduced uranium species, will integrate features of the spectra from the experimental sample as well as of the U(IV) standard. As a consequence, the extracted spectrum will be similar to the U(IV) standard but not necessarily identical. The idea is that the component used to calculate the relative concentration of U(IV) in the samples approximates the average spectrum of U(IV) in the samples; this provides a more robust estimation of the extent of U(VI) reduction than that obtained by linear combination fitting in the case that the correct endmember spectra are not fully identical with those of analyzed reference materials. The U(IV) standard was produced by reducing U(VI) with Ti(III) in acidic solution and precipitating the solid in the presence of silica gel by adding NaOH. In this standard, U(IV) occurs predominately as a coprecipitate with titanium oxide. In the ITT of the XANES spectra, the relative concentration of the second component

DOI: 10.1021/acs.est.6b05453
Environ. Sci. Technol. 2017, 51, 2140−2150

was constrained to one for the U(IV) standard. The concentration of the first component was set to one for the spectrum of U(VI) adsorbed onto hematite. The fitting of the EXAFS spectra was done with the program Artemis.[54] Fourier transformation was performed on the EXAFS spectrum over the k-range between 2 and 11.5 Å with a Hanning window with a sill width of 1.0 Å. The optimization of the fitting parameters took place by simultaneously fitting EXAFS spectra with k-weights of 1, 2, and 3. Details about the fitting strategy can be found in the Supporting Information (SI).

2.5. Reoxidation Experiments. After the 72 h of reaction with sulfide, lepidocrocite suspensions L1, L2, and L3 were brought outside the glovebox, in sealed vessels. Reoxidation was initiated by bubbling air into the vigorously stirred suspensions using air pumps. Although the air was conveyed through gas washing bottles filled with demineralized water, some evaporation was noticed after ~100 h of bubbling. The pH was monitored throughout the two-week duration of the reoxidation experiments and was always around pH 8.0. This implies that dissolution of atmospheric CO_2 did not change the pH considerably in the buffered solution. At pH 8, equilibrium with atmospheric CO_2 pressure corresponds to a dissolved inorganic carbon concentration of about 0.8 mM. The same sample collection procedure was followed as described in section 2.3. Solid samples for XAS analysis were collected after 2 weeks of reoxidation time. XAS samples were prepared and analyzed as described in section 2.4. Reoxidation experiments were not performed for hematite suspensions H1, H2 & H3, due to the limited amount of available material, which was dedicated to the preparation of XAS samples.

3. RESULTS AND DISCUSSION

3.1. Sulfide Reaction with Lepidocrocite and Hematite. Trends of $S(-II)_{aq}$ consumption as a function of time are consistent with those observed in past studies with lepidocrocite[31,33,35,45,56] and hematite.[32,33] In experiments with lepidocrocite (L1, L2, L3), the decrease in concentrations of $S(-II)_{aq}$ was very rapid, with ~98% of added $S(-II)_{aq}$ consumed within the first 30 min of reaction (Figure 1a), beyond which the $S(-II)_{aq}$ concentrations gradually dropped to less than 0.1 mM after 1 h and were undetectable from 6 h to the end of the experiments (72 h in total). Upon addition of $S(-II)_{aq}$ to hematite suspensions (H1, H2, H3), about 50% of $S(-II)_{aq}$, was removed from solution within the first 30 min (Figure 1b). In experiments where $S(-II)_{aq}$ was added in concentrations of 1 (H3) and 5 mM (H2), $S(-II)_{aq}$ values dropped to ~0.5 mM after 3 h but remained above 0.1 mM even after 24 h. In the 10 mM $S(-II)_{aq}$ experiment with hematite (H1), $S(-II)_{aq}$ concentrations decreased to ~3 mM within the first 3 h and remained constant at about 2.5 mM until 24 h (data not shown).

The initial amounts $S(-II)_{aq}$ were insufficient to cause complete consumption of hematite according to the idealized stoichiometry of FeS(s) formation by hematite sulfidization:[33]

$$0.5Fe_2O_3 + 1.5HS^- + 1.5H^+ \Leftrightarrow FeS(s) + \frac{1}{16}S_8^0 + 1.5H_2O \quad (1)$$

Hence, in all three hematite suspensions, the significantly higher $S(-II)_{aq}$ observed after 24 h of reaction time reflects slower reaction kinetics with hematite compared to lepidocrocite. Given that the interfacial areas of the two iron minerals are about the same, the notable difference in $S(-II)_{aq}$ consumption kinetics is due to the intrinsically lower reactivity of hematite. This is in agreement with previous studies on sulfide reaction with iron oxides.[32,33,46,58] For instance, Poulton et al.[33] report surface-normalized rate constants for S(-II) consumption that are about eight times lower for hematite than for lepidocrocite. The observed difference in reaction progress after 30 min is in the same order of magnitude range. The slowdown of reaction kinetics in the hematite suspensions is presumably due to the passivation of the surface layer of the hematite grains similar to that observed during the sulfidization of lepidocrocite.[35]

3.2. Uranium Mobilization by Sulfide. In all the suspensions of lepidocrocite and hematite, the introduction of $S(-II)_{aq}$ was followed by an instantaneous release of adsorbed U into solution (Figure 1c and d). Prior to sulfide addition, aqueous uranium concentrations (U_{aq}) in the lepidocrocite suspensions (L1, L2, L3) were about 1−2 nM, as observed in our previous study.[45] After addition of $S(-II)_{aq}$, U_{aq} concentrations rose to maximum values of about 0.3, 0.2, and 0.09 μM in suspensions L1, L2 and L3, respectively (Figure 1c). That is, the release of U_{aq} correlated with the amounts of $S(-II)_{aq}$ added. The instantaneous release of uranium can be explained by the replacement of ≡Fe−OH groups at the lepidocrocite surface by ≡Fe-SH groups:[45]

$$\equiv Fe - O - UO_2^+ + SH^- + 2H^+ = \equiv Fe - SH + UO^{2+} + H_2O \quad (2)$$

The formation of ≡Fe-SH surface groups through ligand exchange between surface bound OH^- and dissolved SH^- represents the first step in the reaction mechanism of sulfidization of iron oxides.[31,32] Hence, adsorption of $S(-II)_{aq}$ removes ≡Fe−OH groups that act as binding sites for U(VI). The observed desorption of U(VI) is a consequence of the lower affinity of U(VI) for ≡Fe-SH sites than for ≡Fe−OH sites, because U(VI), as a hard acid, more strongly binds to O(-II) than S(-II).[59]

After reaching their maxima within the first 10−15 min, the U_{aq} concentrations in the two lepidocrocite suspensions with the highest $S(-II)_{aq}$ additions, L1 and L2, decreased again (Figure 1c). The largest drop in U_{aq} occurred within the first 30 min, that is, at the same time that most $S(-II)_{aq}$ was consumed (Figure 1a). While the removal of U_{aq} may in part be ascribed to the diminishing competition of $U(VI)_{aq}$ by $S(-II)_{aq}$ for ≡Fe−OH sites,[45] a more important process was likely the reduction of U(VI) into U(IV) (see next section). Beyond the first hour of reaction, and until the end of the experiment (72 h), U_{aq} concentrations stabilized at levels between 0.05 and ~0.1 μM (Figure 1c). These concentrations were higher than the initial levels of U_{aq} in solution, implying that the release of uranium upon $S(-II)_{aq}$ addition was not completely reversible, which is expected as oxygen surface sites are depleted during the sulfidization of lepidocrocite into iron sulfide.[35]

In the hematite suspensions, U_{aq} concentrations were about 1−5 nM prior to $S(-II)_{aq}$ addition. Similar to the experiments with lepidocrocite, instant release of adsorbed U was observed when sulfide was added, but the response was much more pronounced. In the first minutes of reaction, U_{aq} reached values of about 4 μM in all three suspensions (H1, H2, H3), irrespective of the amount of $S(-II)_{aq}$ added (Figure 1d). The maximum U_{aq} concentration were equivalent to ~30% of the total uranium in the suspensions, and surpassed the

DOI: 10.1021/acs.est.6b05453
Environ. Sci. Technol. 2017, 51, 2140−2150

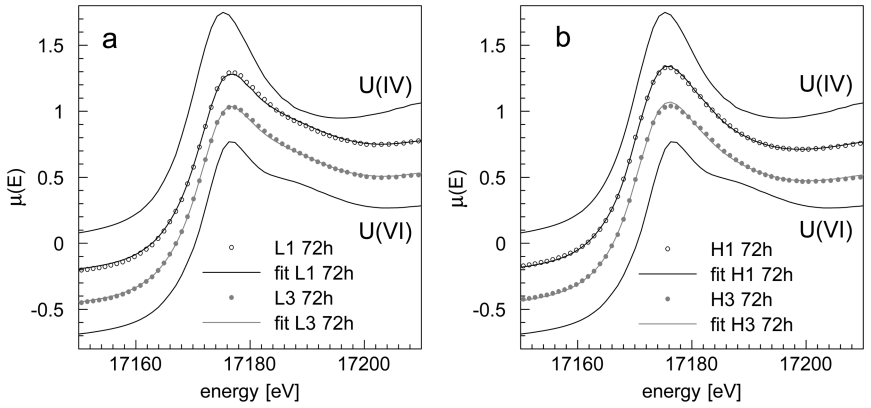

Figure 2. XANES spectra collected at the U L_{III} edge for (a) lepidocrocite and (b) hematite. The dots are spectra collected from the solids of the sulfidization experiments and the lines are the reproduction of the spectra by using two components in the eigenanalysis. XANES spectra of reference materials are U(VI) adsorbed onto hematite and U(IV) that was produced by reducing U(VI) with Ti(III) in acidic solution, which was then precipitated together with the dissolved titanium in the presence of SiO_2 by addition of base.

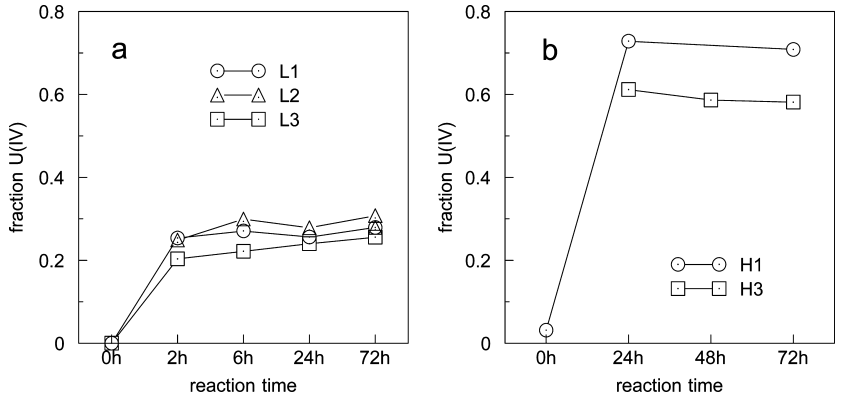

Figure 3. (a, b): Fractions of U(IV) as derived from ITT analysis in (a) lepidocrocite suspensions (L1, L2, L3) in time intervals of 0 (before S(-II) addition), 2, 6, 24, and 72 h of reaction time with S(-II) and (b) hematite suspensions (H1 & H3) in time intervals of 0 (before S(-II) addition), 24, 48, and 72 h of reaction time with S(-II). Note, the *x*-axis in panel a is not linear.

corresponding maximum concentrations in the lepidocrocite suspensions by more than a factor of 10.

The enhanced release of adsorbed U(VI) from hematite is most likely caused by slower S(-II) oxidation kinetics. With lepidocrocite, adsorption of S(-II) is quickly followed by electron transfer and, subsequently, the creation of new surface sites.[35,57] These surface sites become available for readsorption of U(VI) once $S(-II)_{aq}$ is depleted. With hematite, sulfide oxidation proceeds at a slower pace, which implies that the regeneration of surface sites is also slower. Consequently, sulfide occupies surface sites for a longer period, formation of FeS at the surface is facilitated, and $S(-II)_{aq}$ is longer available in solution to compete with U(VI) for adsorption sites. Together, these factors explain why $S(-II)_{aq}$ addition released much more adsorbed U(VI) from hematite than lepidocrocite.

Another difference with the lepidocrocite experiments is that the maximum value of U_{aq} in the hematite suspensions was independent of the amount of $S(-II)_{aq}$ added (Figure 1b). Possibly, the released 4 μM of U(VI) reflect the fraction of adsorbed U(VI) more weakly bound to the hematite surface. The existence of weak and strong binding sites for U(VI) adsorption onto hematite,[60,61] and other iron oxides such as ferrihydrite,[10] has been invoked in surface complexation models. However, to our knowledge, there is no direct spectroscopic evidence for the coexistence of U(VI) complexes with distinct coordination at iron oxide surfaces. In most EXAFS studies only one type of uranium coordination (inner sphere complex) is considered in the structural model for U(VI) adsorbed onto iron oxides in the absence of carbonate.[10,13,60,61]

Competition for ≡Fe−OH sites by $S(-II)_{aq}$ alone does not explain the time evolution of U_{aq} concentrations in the hematite suspensions. Although U_{aq} trends (Figure 1d) resemble those of $S(-II)_{aq}$ (Figure 1b), they are not directly correlated. For example, in the case of H1, U_{aq} concentrations reached ∼0.5 μM after 24 h of reaction. At this time, the $S(-II)_{aq}$ concentration was about 2.5 mM, that is, more than twice the $S(-II)_{aq}$ concentration added to experiment H3 which also caused a maximum U_{aq} release of 4 μM. Thus, other processes contribute to the postmaximum reassociation of U to the solid phase, in particular the reduction of U(VI) to U(IV). By the end of the experiments (72 h), U_{aq} concentrations in all three hematite suspensions had decreased to values of 0.1−0.2 μM, similar to the levels detected at the end of the experiments with lepidocrocite. However, as discussed in the next section, the relative contributions of U(VI) readsorption and U(VI) reduction differed between the lepidocrocite and hematite suspensions.

3.3. Uranium Reduction. *3.3.1. XANES Analyses.* The XANES spectra collected at the U L_{III} edge showed changes upon addition of $S(-II)_{aq}$ that are characteristic of U(VI) reduction to U(IV): (a) a shift of the edge position to lower

DOI: 10.1021/acs.est.6b05453
Environ. Sci. Technol. 2017, 51, 2140−2150

Table 2. Optimized Values for the Different Path Parameters Obtained from EXAFS Modeling for U(VI) Adsorbed onto Lepidocrocite and Hematite

	H1 0h			L3 0h		
sample	N	R_{fit} [Å]	σ^2[Å^2]	N	R_{fit} [Å]	σ^2[Å^2]
U→O_{ax} [a]	2 [b]	1.79 ± 0.02	0.003 ± 0.001	2 [b]	1.79 ± 0.01	0.002 ± 0.001
U→O_{eq}1	2.79 ± 0.37	2.27 ± 0.05	0.004 [b]	3.18 ± 0.36	2.28 ± 0.02	0.004 [b]
U→O_{eq}2	2.21 ± 0.37	2.45 ± 0.07	0.004 [b]	1.82 ± 0.36	2.47 ± 0.05	0.004 [b]
U→O3	0.49 ± 0.75	2.81 ± 0.11	0.004 [b]	1.29 ± 0.88	2.84 ± 0.04	0.004 [b]
U→Fe	1 [b]	3.38 ± 0.06	0.010 ± 0.006	1 [b]	3.33 ± 0.09	0.015 ± 0.013

[a]The model included the multiscattering paths: U → O_{ax},1 → U→O_{ax},1 with $\sigma^2 = 4\sigma^2$ (U → O_{ax}) and $R = 2R$(U → O_{ax}); U → O_{ax},1 → U→O_{ax},2 with $\sigma^2 = 2\sigma^2$ (U → O_{ax}) and $R = 2R$(U → O_{ax}); U → O_{ax},1→ O_{ax},2 →U with $\sigma^2 = 2\sigma^2$ (U → O_{ax}) and $R = 2R$(U → O_{ax}). [b]Fixed values.

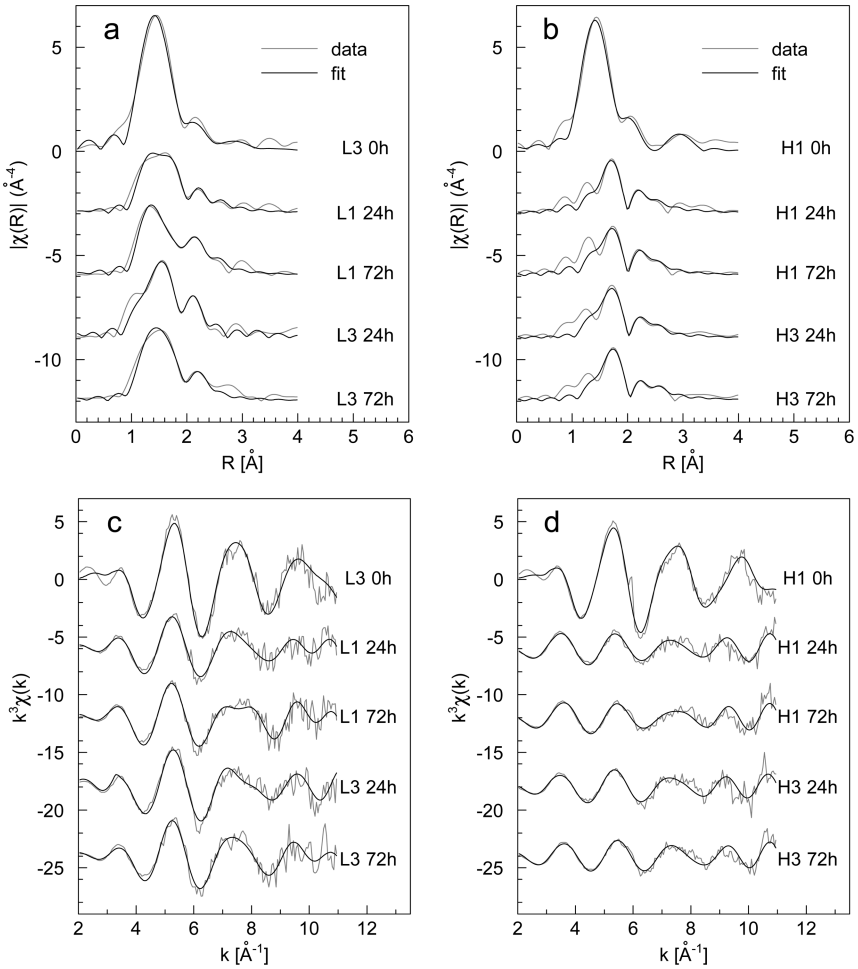

Figure 4. (a−d):k^3-weighted EXAFS spectra (c,d) and their Fourier transformation of samples from experiments with (a,c) lepidocrocite (L1 and L3) and (b,d) hematite (H1 and H3), at 0 (prior to S(-II) addition), 24 and 72 h of reaction time with S(-II). The gray lines are data and the smooth lines are the fitting results.

energies, (b) an increase of the white line intensity, and (c) the disappearance of the characteristic "shoulder" of the U(VI) spectra at the high energy side of the main peak (Figure 2). Eigenanalysis revealed that more than 98% of the variance among all XANES spectra can be explained by the use of two factors. The samples' scores for the two components can be interpreted as an indicator for the extent of U(IV) reduction into U(VI) in the samples. The relative concentrations of U(IV) and U(VI) in the solids was determined by ITT-analysis after expanding the data set with the spectrum of the U(IV) reference material.

Addition of S(-II)$_{aq}$ caused reduction of U(VI) into U(IV) in all iron oxide suspensions (Figure 3). The reduction from U(VI) to U(IV) occurred during the early stages of reaction with S(-II)$_{aq}$. No further reduction of U(VI) took place beyond 24 h. In the case of lepidocrocite, U(IV) reached a maximum equivalent to about 25% of U_{tot} by the second hour of reaction with S(-II)$_{aq}$, with very little increase over the next 3 days (Figure 3a). This was observed in all three lepidocrocite suspensions despite the different added concentrations of S(-II)$_{aq}$. Variable amounts of S(-II)$_{aq}$ also had little effect on the maximum levels of U(IV) produced in the hematite suspensions (Figure 3b). However, for the same added S(-

DOI: 10.1021/acs.est.6b05453
Environ. Sci. Technol. 2017, 51, 2140−2150

II)$_{aq}$ concentrations and the same experimental time frame, the suspensions with hematite yielded much higher percentages of U(IV) than those with lepidocrocite: ~ 70% in H1 and ~60% in H3.

Comparison of U(IV) production in the experiments with hematite and lepidocrocite supports the conclusion of our previous study[45] that reduction of U(VI) is most efficient when S(-II)$_{aq}$ was above the detection limit and U(VI)$_{aq}$ concentrations were elevated. Dissolved sulfide has been shown to reduce U(VI)$_{aq}$ in homogeneous solutions in a matter of hours.[41] However, the measured U(VI)$_{aq}$ concentrations only represent less than 2.5% or 30% of the total uranium in the experiments with lepidocrocite and hematite, respectively. These percentages are smaller than those of formed U(IV), implying that homogeneous reduction of dissolved U(VI) by S(-II) cannot account for U(VI) reduction alone. Reduction of U(VI) by S(-II) can be surface catalyzed[39] but it is also possible that the S$^{\bullet}$ radical,[32] which forms intermediately upon an one electron transfer from S(-II) to Fe(III), is the most potent reductant for U(VI) during iron oxide sulfidization. However, upon reaction with S(-II), the suspensions may contain also a variety of potential reductants of U(VI) in addition to S(-II)$_{aq}$, including amorphous FeS,[44] FeS_2,[42,43,62,63] adsorbed Fe^{2+},[17,18,64] and mixed valence iron oxides, such as magnetite.[35,65] Elemental sulfur is the main product of S(-II) oxidation by Fe oxides[42,44] but formation of surface polysulfides has also been reported.[66] Polysulfides can form complexes with uranyl[67−69] and therefore, reduction of U(VI) might become inhibited due the formation of uranyl−polysulfide complexes.

If reactions between U(VI) and S(-II)$_{aq}$ are the primary pathway generating U(IV), this implies that consumption of S(-II)$_{aq}$ should inhibit U(VI) reduction. Therefore, the conditions favoring U(VI) reduction were only present during the first 2 h in the experiments with lepidocrocite, while they lasted for more than 24 h in the hematite suspensions. The greater extent of U(VI) reduction in the experiments with hematite, can thus be explained by two reasons: (a) addition of S(-II)$_{aq}$ leads to a more extensive release of adsorbed U(VI) to solution, and (b) consumption of S(-II)$_{aq}$ proceeds over a longer period of time due to the slower sulfidization kinetics of hematite. In other words: hematite is a weaker oxidant of S(-II) than lepidocrocite and, consequently, U(VI) initially adsorbed onto hematite is preferentially reduced over U(VI) initially adsorbed onto lepidocrocite.

3.3.2. EXAFS Analyses. The EXAFS spectra of the starting materials, with U(VI) adsorbed onto lepidocrocite and hematite, can be reproduced by a model of an uranyl ion forming a mononuclear bidentate complex with Fe. In this complex, U is bound to two axial (O_{ax}) and five equatorial (O_{eq}) oxygen atoms. The binding distance of U with two of the O_{eq} that connect the uranyl ion to the Fe center is longer than that with the other O_{eq}. The optimized values for the parameters of the model (Table 2 and SI Table 1), are in agreement to those reported in other studies on surface complexes of U(VI) with Fe oxides.[70] The quality of the fitting was improved by adding a fourth O-shell with an optimized distance of 2.81 and 2.84 Å for hematite and lepidocrocite, respectively. In earlier studies, additional oxygen atoms with a comparable distance of 2.87 Å from U have been included when fitting EXAFS spectra of U(VI) adsorbed onto Fe oxides; they have been interpreted as oxygen atoms belonging to the coordinating FeO_6 octahedron.[71]

Changes in U redox state and speciation following the addition of sulfide to the suspensions of lepidocrocite and hematite are also reflected in the k^3-weighted EXAFS spectra and their corresponding Fourier transformation (Figure 4a−d). The indicator function, which is obtained from the eigenanalysis of all k^3-weighted EXAFS spectra, has a minimum for two factors, implying that only two primary factors account for the variation between all spectra, while the remaining variance is primarily caused by experimental noise. The two components extracted by ITT analysis resemble the EXAFS spectra of U(VI) adsorbed onto Fe oxides and the average of all EXAFS spectra from the hematite suspensions after sulfide addition. This suggests that the quality of the EXAFS spectra only allows us to interpret the most pronounced features, which are related to the closest neighboring atoms. For this reason, U−O paths from the optimized model for adsorbed U(VI) were utilized as the starting point in the applied model; an additional O-shell was then added to account for the U−O coordination of reduced uranium. Several attempts were made to exchange O for S in the model but these did not lead to satisfactory fitting results, implying that U is not directly coordinated with S in the samples.

The results obtained from optimizing the model reflect, in the first instance, the reduction of U(VI) to U(IV). The decrease in the amplitude of oscillations between 4 and 10 Å^{-1} in the EXAFS spectra (Figure 4 c and d) can be attributed to the decreased contribution of the U−O_{ax} scattering path, which is characteristic for the uranyl ion. Taking the number of atom pairs of U and axial oxygen atoms (O_{ax}) as an indicator for the extent of U(VI) reduction, the EXAFS results confirm the general trend of more extensive U reduction in the experiments with hematite. The EXAFS spectra similarly did not indicate further U(IV) reduction after 24 h of reaction time. However, the fractions of U(VI) calculated from the optimized O_{ax} coordination number (CN) tend to be smaller than the corresponding fractions obtained from XANES. This difference could be explained by the incorporation of U(VI) or U(V) into the iron oxide lattice, which is reflected in an U−O shell with optimized U−O distances between those for U−O_{ax} and U−O_{eq} of adsorbed U(VI).[14,72] Exposure of iron oxides to reducing conditions can induce recrystallization of iron oxides and the incorporation of previously adsorbed U(VI)[15,16] and its subsequent reduction to U(V).[72]

Reduction of U(VI) to U(IV) is generally expected to result in the precipitation of UO_2. Nonetheless, nonuraninite U(IV) has been identified as a product of microbial[73−77] and abiotic reduction of U(VI).[19,78] In microbial experiments, the preferential formation of nonuraninite U(IV) has been attributed to biological factors,[73] differences in U reduction mechanisms between different bacterial species,[76] and the presence of phosphorus (P) in the form of phosphate[78] or P-bearing ligands[74−76] that appear to inhibit UO_2 formation. The latter implies that complexation of U(IV) might interfere with UO_2 precipitation. Our previous study with lepidocrocite[45] showed that repeated additions of S(-II)$_{aq}$ enhance the extent of U(VI) reduction, ultimately leading to the formation of UO_2, but only when S(-II) is added in sufficient excess. Here, the EXAFS spectra of the lepidocrocite and hematite suspensions did not reveal any U−U scattering peaks, which are characteristic of UO_2 formation (see SI for details). Furthermore, with only a single, initial addition of S(-II)$_{aq}$, incomplete U(VI) reduction was achieved and the produced U(IV) remained in a monomeric state. Even in the case of

DOI: 10.1021/acs.est.6b05453
Environ. Sci. Technol. 2017, 51, 2140−2150

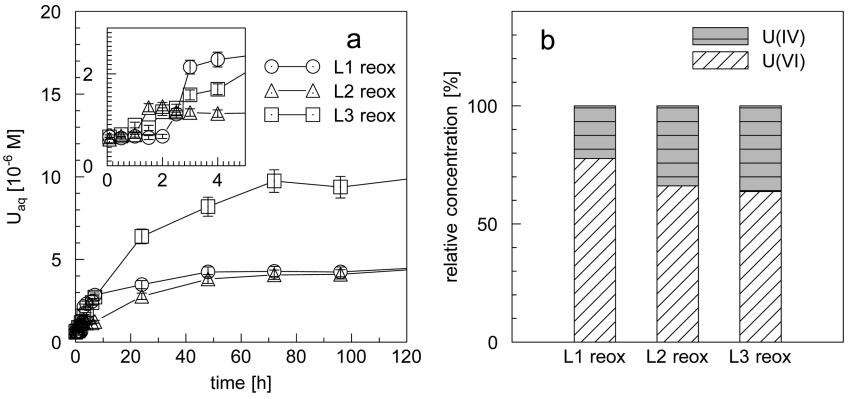

Figure 5. (a,b): (a) Concentrations of U_{aq} from sulfide-reduced suspensions of U-bearing lepidocrocite (L1, L2 & L3) during their exposure to atmospheric air. Error bars present a 7% coefficient of variation. Inlet graph was added to provide a clearer view of the first 5 h of the reoxidation process; (b) shows the relative concentrations of U(VI) and U(IV) obtained from ITT analysis of XANES spectra collected from solids retrieved after 14 days of exposure to atmospheric oxygen.

hematite, where more of the U(VI) was reduced to U(IV) because of the prolonged presence of $S(-II)_{aq}$, there were no indications for UO_2 formation.

3.4. Reoxidation. After 72 h of reaction with S(-II), the lepidocrocite suspensions were exposed to air. Following a lag time of about 2 h, U release to solution proceeded rapidly within the first 10 h of aeration and then continued at a slower, but sustained, pace for the entire 350 h of aeration (Figure 5a). The highest U release was observed for suspension L3, which had been exposed to the lowest level of $S(-II)_{aq}$ (1 mM). In L3, almost all U that had been initially added to the lepidocrocite suspension was recovered in solution after 3 days of reoxidation; this included not only the adsorbed U(VI) but also U(IV), which had formed during sulfidization but was then reoxidized and desorbed. The latter follows the trend of earlier results on the oxidation of bacterially produced monomeric U(IV), which can be brought into solution in the presence of aqueous carbonate within hours.[79,80] In contrast, U released to solution upon aeration only reached approximately 50% of U_{tot} for suspensions L1 and L2, which had reacted with higher amounts of sulfide (10 and 5 mM, respectively). Hence, U release was lower in experiments L1 and L2 in comparison to experiment L3, despite the fraction of U(IV) being comparable in all three suspensions after sulfidization (Figure 3a).

The ITT analysis of the XANES spectra (Figure 5b) indicates that the fraction of solid-phase U(IV) in L1 and L2 increased from about 25% at the start of aeration to 37% and 34%, respectively, by then end of the reoxidation experiments. That is, the solids became relatively enriched in U(IV) during reoxidation. This U(IV) enrichment can be attributed to the preferential desorption of U(VI), which is enhanced by the formation of aqueous U(VI)-carbonate complexes that form due to the introduction of atmospheric CO_2. When accounting for the loss to solution of solid-bound uranium during reoxidation, about 75% (L1) and 87% (L2) of solid-bound U(IV) produced by the end of the sulfidization experiment was still present after 2 weeks exposure to atmospheric oxygen. Thus, it would appear that during sulfidization part of the U(IV) became strongly bound into the Fe mineral transformation products, hence protecting the reduced U from oxidation and remobilization.

Additionally, U(VI) adsorption seems not to be completely reversible in suspensions L1 and L2; part of the solid-bound U(VI) does not undergo desorption and might also become incorporated into iron oxides that may form upon iron sulfide oxidation in a similar way as reported during iron oxide precipitation[14] or induced recrystallization.[15,16] In this case, iron mineral transformations induced by a cycle of sulfidization and reoxidation of iron oxides might be accompanied by U incorporation similarly as reported by microbially driven redox cycling of iron.[16] In suspension L3 the extent of sulfidization was less due to the smaller amounts of sulfide used; this lead to a larger fraction of lepidocrocite still remaining unaltered in suspension. Thus, the effects of mineral transformation in L3 were minimum compared to those in suspensions L1 and L2, leading to an almost complete recovery of U(VI).

4. ENVIRONMENTAL IMPLICATIONS

This study has focused on a parameter that connects sulfidization kinetics with iron oxide mineralogy but which may have gone unnoticed with respect to U behavior: the reactivity of iron oxide minerals toward sulfide. Specifically, competition by $S(-II)_{aq}$ for sites on the iron oxide surfaces mobilized U to solution and the amounts of U released differed greatly between lepidocrocite and hematite. In addition to that, the slower kinetics of reaction between hematite and S(-II) resulted in a much larger conversion of U(VI) into U(IV) than for lepidocrocite. Thus, the resulting iron mineral transformation greatly influences U mobility.

Our findings are of interest when investigating the behavior of uranium and iron mineralogy in sulfur-rich reducing environments, such as coastal marine sediments or flooded acid sulfate soils where available sulfide is often present and sulfidization of iron oxides occurs.[81−85] Sulfidization of iron oxides is also a common process in many terrestrial subsurface environments with high electron donor supply, for example, within landfill plumes.[86] In natural systems, however, the presence of carbonate must be considered as the formation of carbonate complexes with U(VI) may hinder the adsorption of U(VI) onto iron oxide surfaces[87] as well as the potential of U(VI) reduction.[41]

Results from this study also have strong implications for U-contaminated sites where remediation strategies use biostimulation to achieve immobilization of U(VI) by reduction to U(IV)[88−91] For example, in a U-contaminated region in Colorado the Fe(III) reduction and U immobilization that was promoted by a first addition of acetate was overturned by a second acetate addition, which enhanced sulfate reduction and

DOI: 10.1021/acs.est.6b05453
Environ. Sci. Technol. 2017, 51, 2140−2150

remobilized U.[88] Despite sulfide accumulation, it is possible that S(-II) production rates did not exceed S(-II) consumption rates by Fe(III) reduction so that desorption of U(VI) was enabled; desorption, however, might have also been generated by an increase in alkalinity associated with the stimulated anaerobic respiration.[92] At this point, our experiments showed that reduction of released U(VI) is possible when dissolved S(-II) is present in the system. When iron oxides with low reactivity dominate the pool of iron oxides, fast increase and prolonging sulfide production rates might be desired in order to facilitate direct reduction of released U(VI). That is, sulfide consumption rates by iron oxides might be relatively low, which promotes desorption of U(VI) but also allows the built up of dissolved S(-II) that may be available for reduction of U(VI). In this case, remediation strategies have to rely on maintaining reducing conditions for long time scales in order to stabilize the formed U(IV). In contrast, for soils that are dominated by iron oxides with a high reactivity toward sulfide, effective reduction of U(VI), during the onset of sulfide production, might be unattainable. That is, consumption rates of sulfide by reactions with these iron oxides might be too high to allow the establishment of sufficient high levels of dissolved sulfide that would remain available for the purposes of U(VI) reduction. In such cases, incorporation of U into iron minerals might be an alternative strategy for U immobilization. Our results suggest that alternating between oxic and sulfidic conditions can result in the incorporation of U, in either or both oxidation states (U(VI), U(IV)), by the transformation products of the initially present Fe oxides. However, further research is required to delineate conditions that would optimize U incorporation of U(VI) and monomeric U(IV) within iron phases that form during alternations between oxic and sulfidic conditions.

■ ASSOCIATED CONTENT

Supporting Information

The Supporting Information is available free of charge on the ACS Publications website at DOI: 10.1021/acs.est.6b05453.

Complementary work that is associated with this present study is provided and includes: 1) Measured concentrations of dissolved Fe(II) from both lepidocrocite and hematite suspensions during the sulfidization process, 2) Details on EXAFS fitting for adsorbed U(VI) prior and after sulfide addition in lepidocrocite and hematite suspensions including real parts of fitted Fourier transforms and a table that presents optimized values for the different path parameters derived from EXAFS modeling uranium in the samples 3) Images from TEM analysis and collected EDX spectra and 4) Adsorption kinetics of U(VI) onto the lepidocrocite surface at pH 8 as well as sorption isotherms of the same system at pH 6 and 8 (PDF)

■ AUTHOR INFORMATION

Corresponding Author

*Phone: +31 30 253 5008; e-mail: valexand@gmail.com.

ORCID

Vasso G. Alexandratos: 0000-0002-8003-4782

Notes

The authors declare no competing financial interest.

■ ACKNOWLEDGMENTS

We thank the team of the DUBBLE beamline at the ESRF, in particular Dr. S. Nikitenko, for their support during the collection of the XAS spectra. The research leading to these results has received funding from the European Union's European Atomic Energy Community's (Euratom) Seventh Framework Programme FP7/2007-2011 under grant agreement n° 212287 (RECOSY project).

■ REFERENCES

(1) Abdelouas, A. Uranium mill tailings: geochemistry, mineralogy, and environmental impact. *Elements* **2006**, *2* (6), 335−341.

(2) Hu, Q. H.; Weng, J. Q.; Wang, J. S. Sources of anthropogenic radionuclides in the environment: a review. *J. Environ. Radioact.* **2010**, *101* (6), 426−437.

(3) Vodyanitskii, Y. N. Chemical aspects of uranium behavior in soils: A review. *Eurasian Soil Sci.* **2011**, *44* (8), 862−873.

(4) Wang, Y.; Frutschi, M.; Suvorova, E.; Phrommavanh, V.; Descostes, M.; Osman, A. A. A.; Geipel, G.; Bernier-Latmani, R. Mobile uranium(IV)-bearing colloids in a mining-impacted wetland. *Nat. Commun.* **2013**, *4*, 2942−2930.

(5) Aieta, E. M.; Singley, J. E.; Trussell, A. R.; Thorbjarnarson, K. W.; McGuire, M. J. Radionuclides in Drinking Water: An Overview. *J. Am. Water Works Assoc.* **1987**, *79* (4), 144−152.

(6) Orloff, K. G.; Mistry, K.; Charp, P.; Metcalf, S.; Marino, R.; Shelly, T.; Melaro, E.; Donohoe, A. M.; Jones, R. L. Human exposure to uranium in groundwater. *Environ. Res.* **2004**, *94* (3), 319−326.

(7) Brugge, D.; deLemos, J. L.; Oldmixon, B. Exposure pathways and health effects associated with chemical and radiological toxicity of natural uranium: a review. *Rev. Environ. Health* **2005**, *20* (3), 177−194.

(8) Schott, A.; Brand, R. A.; Kaiser, J.; Schmidt, D. Depleted Uranium (DU) — Chemo- and Radiotoxicity. In *Uranium in the Environment: Mining Impact and Consequences*; Merkel, B. J., Hasche-Berger, A., Eds.; Springer: Berlin Heidelberg, 2006; pp 165−174.

(9) Ho, C. H.; Miller, N. H. Adsorption of uranyl species from bicarbonate solution onto hematite particles. *J. Colloid Interface Sci.* **1986**, *110* (1), 165−171.

(10) Waite, T. D.; Davis, J. A.; Payne, T. E.; Waychunas, G. A.; Xu, N. Uranium(VI) Adsorption to Ferrihydrite − Application of a surface complexation model. *Geochim. Cosmochim. Acta* **1994**, *58* (24), 5465−5478.

(11) Bargar, J. R.; Reitmeyer, R.; Lenhart, J. J.; Davis, J. A. Characterization of U(VI)-carbonato ternary complexes on hematite: EXAFS and electrophoretic mobility measurements. *Geochim. Cosmochim. Acta* **2000**, *64* (16), 2737−2749.

(12) Giammar, D. E.; Hering, J. G. Time scales for sorption-desorption and surface precipitation of uranyl on goethite. *Environ. Sci. Technol.* **2001**, *35* (16), 3332−3337.

(13) Sherman, D. M.; Peacock, C. L.; Hubbard, C. G. Surface complexation of U(VI) on goethite (α-FeOOH). *Geochim. Cosmochim. Acta* **2008**, *72* (2), 298−310.

(14) Duff, M. C.; Coughlin, J. U.; Hunter, D. B. Uranium co-precipitation with iron oxide minerals. *Geochim. Cosmochim. Acta* **2002**, *66* (20), 3533−3547.

(15) Nico, P. S.; Stewart, B. D.; Fendorf, S. Incorporation of oxidized uranium into Fe (hydr)oxides during Fe(II) catalyzed remineralization. *Environ. Sci. Technol.* **2009**, *43* (19), 7391−7396.

(16) Stewart, B. D.; Nico, P. S.; Fendorf, S. Stability of uranium incorporated into Fe (hydr)oxides under fluctuating redox conditions. *Environ. Sci. Technol.* **2009**, *43* (13), 4922−4927.

(17) Liger, E.; Charlet, L.; Van Cappellen, P. Surface catalysis of uranium(VI) reduction by iron(II). *Geochim. Cosmochim. Acta* **1999**, *63* (19−20), 2939−2955.

(18) Charlet, L.; Silvester, E.; Liger, E. N-compound reduction and actinide immobilisation in surficial fluids by Fe(II): the surface $\equiv Fe^{III}OFe^{II}OH^{\circ}$ species, as major reductant. *Chem. Geol.* **1998**, *151*, 85−93.

(19) Latta, D. E.; Boyanov, M. I.; Kemner, K. M.; O'Loughlin, E. J.; Scherer, M. M. Abiotic reduction of uranium by Fe(II) in soil. *Appl. Geochem.* **2012**, *27* (8), 1512−1524.
(20) O'Loughlin, E. J.; Kelly, S. D.; Cook, R. E.; Csencsits, R.; Kemner, K. M. Reduction of Uranium(VI) by mixed iron(II/iron(III) hydroxide (green rust): Formation of UO(2) nanoparticles. *Environ. Sci. Technol.* **2003**, *37* (4), 721−727.
(21) Wan, J.; Tokunaga, T. K.; Brodie, E.; Wang, Z.; Zheng, Z.; Herman, D.; Hazen, T. C.; Firestone, M. K.; Sutton, S. R. Reoxidation of bioreduced uranium under reducing conditions. *Environ. Sci. Technol.* **2005**, *39* (16), 6162−6169.
(22) Spycher, N. F.; Issarangkun, M.; Stewart, B. D.; Sengoer, S. S.; Belding, E.; Ginn, T. R.; Peyton, B. M.; Sani, R. K. Biogenic uraninite precipitation and its reoxidation by iron(III) (hydr)oxides: A reaction modeling approach. *Geochim. Cosmochim. Acta* **2011**, *75* (16), 4426−4440.
(23) Ginder-Vogel, M.; Criddle, C. S.; Fendorf, S. Thermodynamic constraints on the oxidation of biogenic UO_2 by Fe(III) (hydr)oxides. *Environ. Sci. Technol.* **2006**, *40* (11), 3544−3550.
(24) Ginder-Vogel, M.; Fendorf, S. Chapter 11: Biogeochemical uranium redox transformations: Potential oxidants of uraninite. In *Developments in Earth and Environmental Sciences*; Mark, O. B.; Douglas, B. K., Eds. Elsevier: Amsterdam, Netherlands, 2007, Vol. *7*, pp 293−319.
(25) Berner, R. A. *Early Diagenesis: A Theoretical Approach*; Princeton University Press: Prinston, NJ, 1980.
(26) Morse, J. W.; Millero, F. J.; Cornwell, J. C.; Rickard, D. The chemistry of the hydrogen sulfide and iron sulfide systems in natural waters. *Earth-Sci. Rev.* **1987**, *24* (1), 1−42.
(27) Widdel, F. Microbiology and ecology of sulfate-and sulfur-reducing bacteria. *Biol. Anaerobic Microorganisms* **1988**, 469−585.
(28) Jørgensen, B. B. The sulfur cycle of a coastal marine sediment (Limfjorden, Denmark). *Limnol. Oceanogr.* **1977**, *22* (5), 814−832.
(29) Raiswell, R.; Berner, R. A. Pyrite formation in euxinic and semi-euxinic sediments. *Am. J. Sci.* **1985**, *285* (8), 710−724.
(30) Canfield, D. E. Reactive iron in marine sediments. *Geochim. Cosmochim. Acta* **1989**, *53* (3), 619−632.
(31) Peiffer, S.; Afonso, M. D.; Wehrli, B.; Gachter, R. Kinetics and mechanism of the reaction of H_2S with lepidocrocite. *Environ. Sci. Technol.* **1992**, *26* (12), 2408−2413.
(32) Dos Santos Afonso, M. D.; Stumm, W. Reductive dissolution of iron(III) (hydr)oxides by hydrogen-sulfide. *Langmuir* **1992**, *8* (6), 1671−1675.
(33) Poulton, S. W.; Krom, M. D.; Raiswell, R. A revised scheme for the reactivity of iron (oxyhydr)oxide minerals towards dissolved sulfide. *Geochim. Cosmochim. Acta* **2004**, *68* (18), 3703−3715.
(34) Poulton, S. W.; Canfield, D. E. Development of a sequential extraction procedure for iron: implications for iron partitioning in continentally derived particulates. *Chem. Geol.* **2005**, *214* (3−4), 209−221.
(35) Hellige, K.; Pollok, K.; Larese-Casanova, P.; Behrends, T.; Peiffer, S. Pathways of ferrous iron mineral formation upon sulfidation of lepidocrocite surfaces. *Geochim. Cosmochim. Acta* **2012**, *81*, 69−81.
(36) Belzile, N.; Tessier, A. Interactions between arsenic and iron oxyhydroxides in lacustrine sediments. *Geochim. Cosmochim. Acta* **1990**, *54* (1), 103−109.
(37) Kocar, B. D.; Borch, T.; Fendorf, S. Arsenic repartitioning during biogenic sulfidization and transformation of ferrihydrite. *Geochim. Cosmochim. Acta* **2010**, *74* (3), 980−994.
(38) Rochette, E. A.; Bostick, B. C.; Li, G.; Fendorf, S. Kinetics of arsenate reduction by dissolved Sulfide. *Environ. Sci. Technol.* **2000**, *34* (22), 4714−4720.
(39) Kochenov, A. V.; Korolev, K. G.; Dubinchuk, V. T.; Medvedev, Y. L. Conditions of Uranium precipitation from water solutions according to experimental data. *Geokhimiya* **1977**, *11*, 1711−1716.
(40) Mohagheghi, A.; Updegraff, D. M.; Goldhaber, M. B. The role of sulfate-reducing bacteria in the deposition of sedimentary uranium ores. *Geomicrobiol. J.* **1985**, *4* (2), 153−173.
(41) Hua, B.; Xu, H.; Terry, J.; Deng, B. Kinetics of uranium(VI) reduction by hydrogen sulfide in anoxic aqueous systems. *Environ. Sci. Technol.* **2006**, *40* (15), 4666−4671.
(42) Wersin, P.; Hochella, M. F.; Persson, P.; Redden, G.; Leckie, J. O.; Harris, D. W. Interaction between aqueous uranium(VI) and sulfide minerals − Spectroscopic evidence for sorption and reduction. *Geochim. Cosmochim. Acta* **1994**, *58* (13), 2829−2843.
(43) Moyes, L. N.; Parkman, R. H.; Charnock, J. M.; Vaughan, D. J.; Livens, F. R.; Hughes, C. R.; Braithwaite, A. Uranium uptake from aqueous solution by interaction with goethite, lepidocrocite, muscovite, and mackinawite: An X-ray absorption spectroscopy study. *Environ. Sci. Technol.* **2000**, *34* (6), 1062−1068.
(44) Hua, B.; Deng, B. Reductive immobilization of uranium(VI) by amorphous iron sulfide. *Environ. Sci. Technol.* **2008**, *42* (23), 8703−8708.
(45) Alexandratos, V. G.; Behrends, T.; Van Cappellen, P. Sulfidization of lepidocrocite and its effect on uranium phase distribution and reduction. *Geochim. Cosmochim. Acta* **2014**, *142*, 570−586.
(46) Peiffer, S.; Gade, W. Reactivity of ferric oxides toward H2S at low pH. *Environ. Sci. Technol.* **2007**, *41* (9), 3159−3164.
(47) Schwertmann, U.; Cornell, R. M. *Iron Oxides in the Laboratory: Preparation and Characterization*, 2nd ed.; Wiley-VCH: Weinheim ; New York, 2000; pp 1−188.
(48) Scherrer, P. Bestimmung der Größe und der inneren Struktur von Kolloidteilchen mittels Röntgenstrahlen. Nachrichten von der Gesellschaft der Wissenschaften zu Göttingen. *Mathematisch-Physikalische* **1918**, 98−100.
(49) Reimers, C. E.; Ruttenberg, K. C.; Canfield, D. E.; Christiansen, M. B.; Martin, J. B. Porewater pH and authigenic phases formed in the uppermost sediments of the Santa Barbara Basin. *Geochim. Cosmochim. Acta* **1996**, *60* (21), 4037−4057.
(50) Stookey, L. L. Ferrozine: a new spectrophotometric reagent for iron. *Anal. Chem.* **1970**, *42* (7), 779−781.
(51) Fonselius, S.; Dyrssen, D.; Yhlen, B. *Determination of Hydrogen Sulphide. Methods of Seawater Analysis*, 3rd ed.; 1976, pp 91−100.
(52) Borsboom, M.; Bras, W.; Cerjak, I.; Detollenaere, D.; Glastra van Loon, D.; Goedtkindt, P.; Konijnenburg, M.; Lassing, P.; Levine, Y. K.; Munneke, B.; Oversluizen, M. The Dutch−Belgian beamline at the ESRF. *J. Synchrotron Radiat.* **1998**, *5* (3), 518−520.
(53) Nikitenko, S.; Beale, A. M.; van der Eerden, A. M.; Jacques, S. D.; Leynaud, O.; O'Brien, M. G.; Detollenaere, D.; Kaptein, R.; Weckhuysen, B. M.; Bras, W. Implementation of a combined SAXS/WAXS/QEXAFS set-up for time-resolved in situ experiments. *J. Synchrotron Radiat.* **2008**, *15* (6), 632−640.
(54) Ravel, B.; Newville, M. ATHENA, ARTEMIS, HEPHAESTUS: data analysis for X-ray absorption spectroscopy using IFEFFIT. *J. Synchrotron Radiat.* **2005**, *12*, 537−541.
(55) Rossberg, A.; Reich, T.; Bernhard, G. Complexation of uranium(VI) with protocatechuic acid - application of iterative transformation factor analysis to EXAFS spectroscopy. *Anal. Bioanal. Chem.* **2003**, *376* (5), 631−638.
(56) Poulton, S. W. Sulfide oxidation and iron dissolution kinetics during the reaction of dissolved sulfide with ferrihydrite. *Chem. Geol.* **2003**, *202* (1−2), 79−94.
(57) Peiffer, S.; Behrends, T.; Hellige, K.; Larese-Casanova, P.; Wan, M.; Pollok, K. Pyrite formation and mineral transformation pathways upon sulfidation of ferric hydroxides depend on mineral type and sulfide concentration. *Chem. Geol.* **2015**, *400*, 44−55.
(58) Canfield, D. E.; Raiswell, R.; Bottrell, S. H. The reactivity of sedimentary iron minerals toward sulfide. *Am. J. Sci.* **1992**, *292* (9), 659−683.
(59) Stumm, W.; Morgan, J. Aquatic Chemistry: Chemical Equilibria and Rates in Natural Waters; John Wiley: New York, 1996; Vol. *126*, pp 1022.
(60) Zeng, H.; Singh, A.; Basak, S.; Ulrich, K. U.; Sahu, M.; Biswas, P.; Catalano, J. G.; Giammar, D. E. Nanoscale Size Effects on Uranium(VI) Adsorption to Hematite. *Environ. Sci. Technol.* **2009**, *43* (5), 1373−1378.

DOI: 10.1021/acs.est.6b05453
Environ. Sci. Technol. 2017, 51, 2140−2150

(61) Hsi, C.-K. D.; Langmuir, D. Adsorption of uranyl onto ferric oxyhydroxides: Application of the surface complexation site-binding model. *Geochim. Cosmochim. Acta* **1985**, *49* (9), 1931−1941.
(62) Livens, F. R.; Jones, M. J.; Hynes, A. J.; Charnock, J. M.; Mosselmans, J. F. W.; Hennig, C.; Steele, H.; Collison, D.; Vaughan, D. J.; Pattrick, R. A. D.; Reed, W. A.; Moyes, L. N. X-ray absorption spectroscopy studies of reactions of technetium, uranium and neptunium with mackinawite. *J. Environ. Radioact.* **2004**, *74* (1−3), 211−219.
(63) Scott, T. B.; Riba Tort, O.; Allen, G. C. Aqueous uptake of uranium onto pyrite surfaces; reactivity of fresh versus weathered material. *Geochim. Cosmochim. Acta* **2007**, *71* (21), 5044−5053.
(64) Fredrickson, J. K.; Zachara, J. M.; Kennedy, D. W.; Duff, M. C.; Gorby, Y. A.; Li, S. M. W.; Krupka, K. M. Reduction of U(VI) in goethite (alpha-FeOOH) suspensions by a dissimilatory metal-reducing bacterium. *Geochim. Cosmochim. Acta* **2000**, *64* (18), 3085−3098.
(65) Behrends, T.; Van Cappellen, P. Transformation of hematite into magnetite during dissimilatory iron reduction - Conditions and mechanisms. *Geomicrobiol. J.* **2007**, *24* (5), 403−416.
(66) Wan, M.; Shchukarev, A.; Lohmayer, R.; Planer-Friedrich, B.; Peiffer, S. Occurrence of surface polysulfides during the interaction between ferric (hydr) oxides and aqueous sulfide. *Environ. Sci. Technol.* **2014**, *48* (9), 5076−5084.
(67) Manos, E.; Kanatzidis, M. G.; Ibers, J. A. *Actinide Chalcogenide Compounds. In The Chemistry of the Actinide and Transactinide Elements*; Morss, L. R., Edelstein, N. M., Fuger, J., Eds.; Springer Netherlands: Dordrecht, 2011; pp 4005−4077.
(68) Manos, M. J.; Kanatzidis, M. G. Layered metal sulfides capture uranium from seawater. *J. Am. Chem. Soc.* **2012**, *134* (39), 16441−16446.
(69) Ma, S.; Huang, L.; Ma, L.; Shim, Y.; Islam, S. M.; Wang, P.; Zhao, L.-D.; Wang, S.; Sun, G.; Yang, X.; Kanatzidis, M. G. Efficient uranium capture by polysulfide/layered double hydroxide composites. *J. Am. Chem. Soc.* **2015**, *137* (10), 3670−3677.
(70) Kelly, S. D.; Balwant, S.; Markus, G. Chapter 14: Uranium Chemistry in Soils and Sediments. In *Developments in Soil Science*; Elsevier, 2010; Vol. *34*, pp 411−466.
(71) Ulrich, K.-U.; Rossberg, A.; Foerstendorf, H.; Zaenker, H.; Scheinost, A. C. Molecular characterization of uranium(VI) sorption complexes on iron(III)-rich acid mine water colloids. *Geochim. Cosmochim. Acta* **2006**, *70* (22), 5469−5487.
(72) Ilton, E. S.; Pacheco, J. S. L.; Bargar, J. R.; Shi, Z.; Liu, J.; Kovarik, L.; Engelhard, M. H.; Felmy, A. R. Reduction of U(VI) incorporated in the structure of hematite. *Environ. Sci. Technol.* **2012**, *46* (17), 9428−9436.
(73) Fletcher, K. E.; Boyanov, M. I.; Thomas, S. H.; Wu, Q.; Kemner, K. M.; Löffler, F. E. U(VI) Reduction to mononuclear U(IV) by Desulfitobacterium Species. *Environ. Sci. Technol.* **2010**, *44* (12), 4705−4709.
(74) Bernier-Latmani, R.; Veeramani, H.; Vecchia, E. D.; Junier, P.; Lezama-Pacheco, J. S.; Suvorova, E. I.; Sharp, J. O.; Wigginton, N. S.; Bargar, J. R. Non-uraninite products of microbial U(VI) reduction. *Environ. Sci. Technol.* **2010**, *44* (24), 9456−9462.
(75) Sharp, J. O.; Lezama-Pacheco, J. S.; Schofield, E. J.; Junier, P.; Ulrich, K.-U.; Chinni, S.; Veeramani, H.; Margot-Roquier, C.; Webb, S. M.; Tebo, B. M.; Giammar, D. E.; Bargar, J. R.; Bernier-Latmani, R. Uranium speciation and stability after reductive immobilization in aquifer sediments. *Geochim. Cosmochim. Acta* **2011**, *75* (21), 6497−6510.
(76) Boyanov, M. I.; Fletcher, K. E.; Kwon, M. J.; Rui, X.; O'Loughlin, E. J.; Löffler, F. E.; Kemner, K. M. Solution and microbial controls on the formation of reduced U(IV) species. *Environ. Sci. Technol.* **2011**, *45* (19), 8336−8344.
(77) Cerrato, J. M.; Ashner, M. N.; Alessi, D. S.; Lezama-Pacheco, J. S.; Bernier-Latmani, R.; Bargar, J. R.; Giammar, D. E. Relative reactivity of biogenic and chemogenic uraninite and biogenic noncrystalline U(IV). *Environ. Sci. Technol.* **2013**, *47* (17), 9756−9763.
(78) Veeramani, H.; Alessi, D. S.; Suvorova, E. I.; Lezama-Pacheco, J. S.; Stubbs, J. E.; Sharp, J. O.; Dippon, U.; Kappler, A.; Bargar, J. R.; Bernier-Latmani, R. Products of abiotic U(VI) reduction by biogenic magnetite and vivianite. *Geochim. Cosmochim. Acta* **2011**, *75* (9), 2512−2528.
(79) Alessi, D. S.; Uster, B.; Veeramani, H.; Suvorova, E. I.; Lezama-Pacheco, J. S.; Stubbs, J. E.; Bargar, J. R.; Bernier-Latmani, R. Quantitative separation of monomeric U(IV) from UO2 in products of U(VI) reduction. *Environ. Sci. Technol.* **2012**, *46* (11), 6150−6157.
(80) Bi, Y.; Stylo, M.; Bernier-Latmani, R.; Hayes, K. F. Rapid mobilization of noncrystalline U(IV) coupled with FeS oxidation. *Environ. Sci. Technol.* **2016**, *50* (3), 1403−1411.
(81) Van Breemen, N. *Genesis, Morphology, and Classification of Acid Sulfate Soils in Coastal Plains1. In Acid Sulfate Weathering*; Kittrick, J. A., Fanning, D. S., Hossner, L. R., Eds.; Soil Science Society of America: Madison, WI, 1982; pp 95−108.
(82) Canfield, D. E. Reactive iron in marine sediments. *Geochim. Cosmochim. Acta* **1989**, *53* (3), 619−632.
(83) Chaillou, G.; Anschutz, P.; Lavaux, G.; Schafer, J.; Blanc, G. The distribution of Mo, U, and Cd in relation to major redox species in muddy sediments of the Bay of Biscay. *Mar. Chem.* **2002**, *80* (1), 41−59.
(84) Powell, B.; Martens, M. A review of acid sulfate soil impacts, actions and policies that impact on water quality in Great Barrier Reef catchments, including a case study on remediation at East Trinity. *Mar. Pollut. Bull.* **2005**, *51*, 149−164.
(85) Burton, E. D.; Bush, R. T.; Sullivan, L. A.; Johnston, S. G.; Hocking, R. K. Mobility of arsenic and selected metals during re-flooding of iron- and organic-rich acid-sulfate soil. *Chem. Geol.* **2008**, *253*, 64−73.
(86) Christensen, T. H.; Kjeldsen, P.; Bjerg, P. L.; Jensen, D. L.; Christensen, J. B.; Baun, A.; Albrechtsen, H.-J. r.; Heron, G. Biogeochemistry of landfill leachate plumes. *Appl. Geochem.* **2001**, *16*, 659−718.
(87) Wazne, M.; Korfiatis, G. P.; Meng, X. Carbonate effects on hexavalent uranium adsorption by iron oxyhydroxide. *Environ. Sci. Technol.* **2003**, *37* (16), 3619−3624.
(88) Anderson, R. T.; Vrionis, H. A.; Ortiz-Bernad, I.; Resch, C. T.; Long, P. E.; Dayvault, R.; Karp, K.; Marutzky, S.; Metzler, D. R.; Peacock, A.; White, D. C.; Lowe, M.; Lovley, D. R. Stimulating the in situ activity of Geobacter species to remove uranium from the groundwater of a uranium-contaminated aquifer. *J. Appl. Environ. Microbiol.* **2003**, *69* (10), 5884−5891.
(89) Dong, W. M.; Xie, G. B.; Miller, T. R.; Franklin, M. P.; Oxenberg, T. P.; Bouwer, E. J.; Ball, W. P.; Halden, R. U. Sorption and bioreduction of hexavalent uranium at a military facility by the Chesapeake Bay. *Environ. Pollut.* **2006**, *142* (1), 132−142.
(90) Wu, W.-M.; Carley, J.; Gentry, T.; Ginder-Vogel, M. A.; Fienen, M.; Mehlhorn, T.; Yan, H.; Caroll, S.; Pace, M. N.; Nyman, J.; Luo, J.; Gentile, M. E.; Fields, M. W.; Hickey, R. F.; Gu, B.; Watson, D.; Cirpka, O. A.; Zhou, J.; Fendorf, S.; Kitanidis, P. K.; Jardine, P. M.; Criddle, C. S. Pilot-scale in situ bioremedation of uranium in a highly contaminated aquifer. 2. Reduction of U(VI) and geochemical control of U(VI) bioavailability. *Environ. Sci. Technol.* **2006**, *40* (12), 3986−3995.
(91) Wu, W.-M.; Carley, J.; Luo, J.; Ginder-Vogel, M. A.; Cardenas, E.; Leigh, M. B.; Hwang, C.; Kelly, S. D.; Ruan, C.; Wu, L.; Van Nostrand, J.; Gentry, T.; Lowe, K.; Mehlhorn, T.; Carroll, S.; Luo, W.; Fields, M. W.; Gu, B.; Watson, D.; Kemner, K. M.; Marsh, T.; Tiedje, J.; Zhou, J.; Fendorf, S.; Kitanidis, P. K.; Jardine, P. M.; Criddle, C. S. In situ bioreduction of uranium (VI) to submicromolar levels and reoxidation by dissolved oxygen. *Environ. Sci. Technol.* **2007**, *41* (16), 5716−5723.
(92) Long, P. E.; Williams, K. H.; Davis, J. A.; Fox, P. M.; Wilkins, M. J.; Yabusaki, S. B.; Fang, Y.; Waichler, S. R.; Berman, E. S. F.; Gupta, M.; Chandler, D. P.; Murray, C.; Peacock, A. D.; Giloteaux, L.; Handley, K. M.; Lovley, D. R.; Banfield, J. F. Bicarbonate impact on U(VI) bioreduction in a shallow alluvial aquifer. *Geochim. Cosmochim. Acta* **2015**, *150*, 106−124.

DOI: 10.1021/acs.est.6b05453
Environ. Sci. Technol. 2017, 51, 2140−2150